Polarization-dependent resonant inelastic x-ray scattering of β-Ga$_2$O$_3$: An experimental and computational study ⓕ

Elizaveta Pyatenko ✉ iD ; John Vinson iD ; Dirk Hauschild iD ; Constantin Wansorra iD ; Wanli Yang iD ;
Monika Blum iD ; Clemens Heske iD ; Lothar Weinhardt ✉ iD

Check for updates

View Online

Export Citation

AIP Publishing

Polarization-dependent resonant inelastic x-ray scattering of β-Ga₂O₃: An experimental and computational study ⓕ

Elizaveta Pyatenko,[1,a),b)] ⓘD **John Vinson,**[2] ⓘD **Dirk Hauschild,**[1,3,4] ⓘD **Constantin Wansorra,**[1,4] ⓘD **Wanli Yang,**[5] ⓘD
Monika Blum,[4,5,6] ⓘD **Clemens Heske,**[1,3,4] ⓘD **and Lothar Weinhardt**[1,3,4,a)] ⓘD

AFFILIATIONS

[1] Institute for Photon Science and Synchrotron Radiation (IPS), Karlsruhe Institute of Technology (KIT), Kaiserstraße 12,
76131 Karlsruhe, Germany
[2] Material Measurement Laboratory, National Institute of Standards and Technology (NIST), Gaithersburg, Maryland 20899, USA
[3] Institute for Chemical Technology and Polymer Chemistry (ITCP), Karlsruhe Institute of Technology (KIT), Kaiserstraße 12,
76131 Karlsruhe, Germany
[4] Department of Chemistry and Biochemistry, University of Nevada, Las Vegas (UNLV), 4505 Maryland Parkway, Las Vegas,
Nevada 89154-4003, USA
[5] Advanced Light Source, Lawrence Berkeley National Laboratory, 1 Cyclotron Road, Berkeley, California 94720, USA
[6] Chemical Sciences Division, Lawrence Berkeley National Laboratory, 1 Cyclotron Road, Berkeley, California 94720, USA

Note: This paper is part of the Special Topic on Ultrawide Bandgap Semiconductors.
a)Authors to whom correspondence should be addressed: pyatenko@post.kek.jp and lothar.weinhardt@kit.edu
b)Current address: Institute of Materials Structure Science (IMSS), High Energy Accelerator Research Organization (KEK), 1-1 Oho,
Tsukuba, Ibaraki 305-0801, Japan.

ABSTRACT

The bulk electronic structure of β-Ga₂O₃ single crystals was investigated using oxygen K-edge x-ray emission and absorption spectroscopy as well as resonant inelastic soft x-ray scattering. Spectra were obtained for different orientations of the crystal planes with respect to the polarization vector of the incident x-ray beam. The spectra are analyzed with calculations based on density functional theory and using the Bethe–Salpeter equation in the OCEAN code to take the core–hole interaction into account. These calculations correctly capture all the main features in the experimental spectra, demonstrating the potential of the approach to predict the electronic properties of similar compounds. We find a pronounced anisotropy as a function of the excitation polarization vector and significant differences in the spectral contributions from the inequivalent oxygen atoms of β-Ga₂O₃.

Ga₂O₃ is an ultra-wide bandgap material,[1] with literature bandgap values ranging from 4.4 to 4.9 eV.[2–8] It can be used as a transparent conductive oxide (TCO), with good electrical conductivity and transparency in the UV–visible light region. Ga₂O₃ has been used in a wide variety of applications:[9] as a buffer[3,10] or intrinsically "high-resistive" layer[11] in Cu(In, Ga)Se₂ (CIGSe)-based thin-film solar cells, in power electronics,[12–15] solar-blind UV detectors,[16–19] gas-sensing devices,[20–22] catalysts,[23,24] and space-based applications.[25,26] A detailed and fundamental understanding of its electronic structure is crucial for further insight-driven optimization of these (and similar) devices.

There are five different polymorphs of crystalline Ga₂O₃, α, β, γ, δ, and ε,[27] with the β polymorph being the most stable under ambient temperature and pressure. The crystal structure of

β-Ga_2O_3 is anisotropic, which is reflected in its electronic and optical properties. Several studies have shown anisotropy in the optical absorption, resulting in different bandgap values depending on the polarization of light.[5,28–30] Angle-resolved photoelectron spectroscopy (ARPES) studies have been performed to determine the band structure and a good correspondence with density functional theory (DFT) calculations was found.[31–34] Cocchi et al. investigated the energy-loss near-edge fine structure (ELNES) at the O K edge of β-Ga_2O_3,[35] together with spectra collected with a transmission electron microscope. By changing the diffraction conditions and comparing with calculations based on the Bethe–Salpeter equation (BSE), information about the inequivalent oxygen atoms could be gathered. Swallow et al. investigated different polymorphs of Ga_2O_3[36] with x-ray absorption spectroscopy (XAS) and found that the spectra vary significantly depending on the polymorph and its crystal structure. Vorwerk et al. studied extensively the theoretical O K, Ga L_2, and Ga K resonant inelastic x-ray scattering (RIXS) spectra of Ga_2O_3,[37,38] and one of the foci was to understand how the absorption spectra differ between the polymorphs. To date, no experimental RIXS studies of Ga_2O_3 have been published.

In this work, the experimental oxygen K x-ray emission spectroscopy (XES), XAS, and RIXS spectra of single crystal β-Ga_2O_3 for three different polarization directions are presented and compared to calculations using DFT and BSE approaches, which correctly reproduce the main features in the experimental spectra. By performing polarization-dependent measurements and calculations, we are able to selectively probe different regions of the band structure of β-Ga_2O_3, as well as enhance or suppress contributions from inequivalent O atoms.

Figure 1 shows the conventional unit cell of β-Ga_2O_3, with two inequivalent Ga atoms: the tetrahedrally coordinated atoms are labeled as Ga1 and the octahedrally coordinated atoms are labeled Ga2. There are also three inequivalent O atoms: O1 has two bonds with Ga2 and one bond with Ga1, O2 has *three* bonds with Ga2 and one bond with Ga1, and O3 has *one* bond with Ga2 and *two* bonds with Ga1. The three inequivalent O atoms contribute differently to the spectra, depending on the polarization of the incident x-ray beam, as we will show in this paper.

As a first step, the non-resonant O K XES spectra of β-Ga_2O_3 are presented in Fig. 2, in comparison with calculations based on DFT and the OCEAN code. According to the final-state rule,[41–43] ground-state calculations are often sufficient to simulate non-resonant XES spectra; all calculations presented in Fig. 2 are
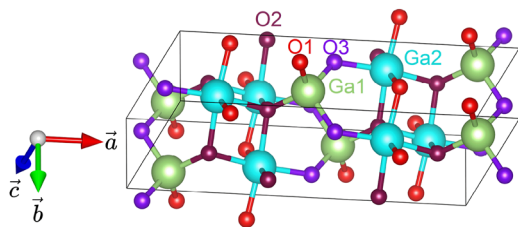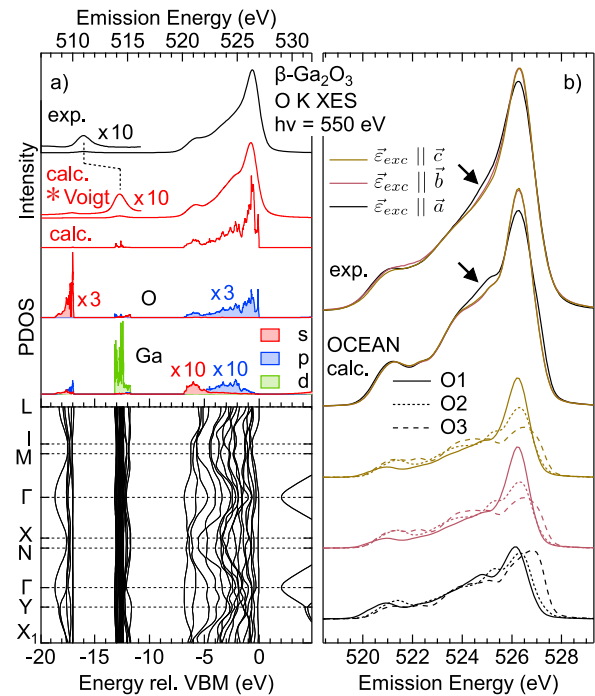
FIG. 2. Comparison of the experimental O K XES spectrum of β-Ga_2O_3 with DFT calculations. (a) From bottom to top: calculated k-resolved band structure; projected density of states (PDOS) for gallium and oxygen; separated in s (red), p (blue), and d (green) symmetry; calculated O K XES spectrum without ("calc.") and with ("calc. ∗ Voigt") experimental and lifetime broadening; and the sum of the experimental XES spectra for the three polarization directions excited with 550 eV photons (black, top). Small spectral contributions are also magnified by the given factors. (b) From bottom to top: spectra calculated using the OCEAN code separated into O1 (continuous line), O2 (short dashed line), and O3 (long dashed line) contributions for $\vec{\varepsilon}_{exc} \parallel \vec{a}$ (black), $\vec{b}$ (red), and $\vec{c}$ (yellow), calculations summed over all oxygen atoms ("OCEAN calc."), and (top) experimental spectra for the three polarization directions (arrows point at the region of largest difference between the spectra). In the experimental spectra and the OCEAN calculation, the contributions for $\vec{b}$ (red) and $\vec{c}$ (yellow) are very similar and lie on top of each other.

thus based on DFT (i.e., a ground-state approach). For the calculations in Fig. 2(a), the Wien2k program package[44] was used. This calculation uses the formalism developed by Schwartz et al. to derive an *angle-integrated* XES spectrum based on the projected density of states (PDOS).[45] As an approximation of an angle-integrated spectrum, we summed up the experimental non-resonant XES spectra for three different polarization directions. The spectra in Fig. 2(b) were calculated for different polarization directions and separated for the inequivalent oxygen atoms using DFT with the OCEAN code.[46,47]

Starting at the bottom of Fig. 2(a), the calculated k-resolved band structure is shown, with the energy relative to the valence band maximum (VBM) on the abscissa and the crystal momentum on the ordinate. The band structure can be divided into three regions: the upper valence band region at 0–7 eV, Ga 3d-derived bands at 12–13 eV, and O 2s-derived bands at 17–20 eV below the VBM, respectively. The atom- and symmetry-resolved PDOS (Ga s, Ga p,

FIG. 1. Conventional unit cell of β-Ga_2O_3 (see Refs. 35 and 39). Tetrahedrally (Ga1) and octahedrally (Ga2) coordinated Ga atoms are represented by green and turquois, respectively. Inequivalent O atoms are represented by red (O1), maroon (O2), and purple (O3). The image was produced using VESTA software.[40]

Ga d, O s, and O p) is shown above the band structure. The upper valence band region is mostly composed of oxygen p orbitals. Moreover, while the Ga 3d-derived bands mostly contribute to the Ga PDOS, small admixtures from O 2s and O 2p states are found in this region as well. In fact, Ga 3d – O 2s[36] as well as Ga 3d – O 2p hybridization (similarly to that observed for other metal oxides[48]) occurs, with a small contribution from Ga 3d to the O 2s-derived bands.

The calculated O K XES spectrum, without and with experimental and lifetime broadening, is shown above the PDOS. Its main peak, approx. −1 eV below the VBM (at an emission energy of ≈526 eV), is dominated by contributions from the O 2p-derived band. In addition, there is a small peak at approx. −13 eV relative to the VBM (≈514 eV emission energy) due to transitions from the Ga 3d-derived band that contains O 2p contributions. The calculation gives a good description of the experimental non-resonant spectrum, with all the main features present. We note that the experimental Ga 3d-derived band appears at almost 5 eV lower emission energy than that in the calculation (indicated by the dotted line). This underestimation of the position of d-bands is well known when using DFT with local density (LDA) or generalized gradient (GGA) approximations (as in the present case).[49]

In the top half of Fig. 2(b), we now compare the experimental emission spectra, for all three polarization directions separately, with the corresponding spectra calculated with OCEAN. Overall, the spectra for the three polarization directions are very similar, both in experiment and calculation. However, the spectrum for the $\vec{\varepsilon}_{exc} \parallel \vec{a}$ direction has a slightly smaller relative intensity of the main peak at 526 eV and exhibits a more intense shoulder at lower energies (≈525 eV, indicated by the black arrows in Fig. 2(b). These differences are accurately reproduced by the calculation. In the bottom half of Fig. 2(b), the calculated XES spectra for the three polarization directions are further separated into contributions from the differently coordinated oxygen atoms (i.e., O1, O2, and O3). The contribution from O3 is stronger in the emission spectrum with $\vec{\varepsilon}_{exc} \parallel \vec{a}$ than for the other two directions. The O3 contribution is shifted toward higher emission energy relative to O1 and O2, explaining the difference in the observed experimental spectrum for the $\vec{\varepsilon}_{exc} \parallel \vec{a}$ direction. Nonetheless, the difference in the emission spectra for the different polarization directions is rather small and not as significant as in the absorption spectra that will be discussed in the following.

Figure 3 shows the experimental (left) and BSE-calculated (right) O K RIXS maps of β-Ga_2O_3 for the three polarization directions. As a function of excitation energy, the overall emission intensities in the maps represent the absorption spectra, which will be discussed in detail in conjunction with Fig. 4. The intensity variations are significantly different for the three different polarization directions and are well-reproduced in the calculations. While the calculated line positions and spectral weights slightly shift along the emission energy axis as a function of excitation energy, this is barely visible in the experimental data. This can be partially attributed to additional experimental broadening in the measurements, as well as the fact that the experimental data also include contributions from processes in which momentum is transferred to phonons or other electrons (henceforth called "incoherent contributions").[50] Such momentum transfers have a wide distribution in k-space, leading to a broadening of the spectra since the experimental spectra are
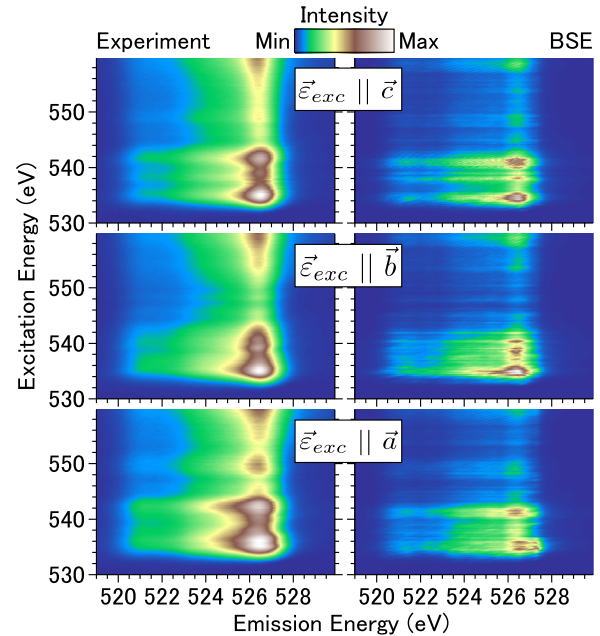
FIG. 3. Experimental (left) and BSE-calculated (right) O K RIXS maps of β-Ga_2O_3 for the three polarization directions: $\vec{\varepsilon}_{exc} \parallel \vec{a}$ (bottom), $\vec{\varepsilon}_{exc} \parallel \vec{b}$ (middle), and $\vec{\varepsilon}_{exc} \parallel \vec{c}$ (top). The color-coded emission intensity is shown as a function of the excitation and emission energies.
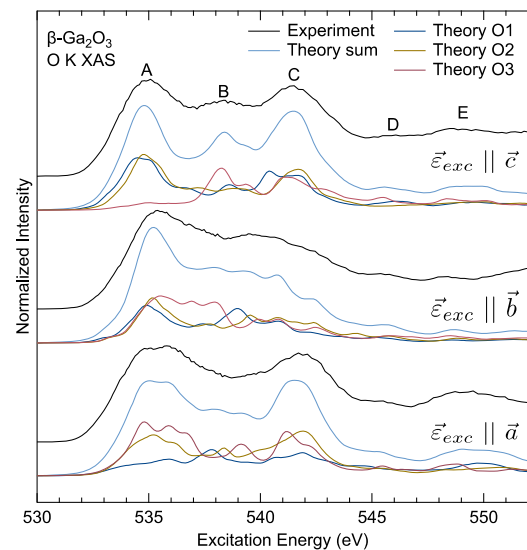
FIG. 4. Comparison of the experimental (black) and calculated (blue, using OCEAN and the BSE approach) XAS spectra for the three polarization directions. In addition to the calculated sum (light blue), calculated spectra are shown for the inequivalent oxygen atoms individually (blue, yellow, and red). All calculated spectra were convoluted with Voigt line profiles to account for experimental and lifetime broadening. The excitation energy axes of all calculated spectra were shifted by the same amount and stretched (by a factor of 1.05) to match the experimental spectra.

then sums of the coherent and incoherent contributions. In contrast, the direction of the photon momentum (whose magnitude corresponds to a sizable portion of the Brillouin zone) is well defined by the orientation of the single crystal and the measurement geometry. The strongest changes in RIXS spectral shape as a function of excitation energy are observed close to the absorption onset (i.e., between excitation energies of 530 and 533 eV). This is due to a higher degree of coherence in this region, as will be discussed in detail in conjunction with Fig. 5.

Figure 4 shows the measured and calculated partial fluorescence yield (PFY) O K XAS spectra of β-Ga_2O_3 for the three polarization directions. The calculated spectra and their dependence on the non-equivalent oxygen atoms and the polarization direction are in good agreement with the results in Ref. 37, where a very similar BSE-based approach was used. The experimental spectra were generated from the RIXS maps in Fig. 3 by integrating the emission intensity between emission energies of 519 and 529 eV for each excitation energy. The spectra were then normalized to the XAS edge jump from 530 to 560 eV. The experimental spectra exhibit several absorption features, labeled A-E, which are enhanced in some polarization directions while reduced in others. These changes, as well as the overall shapes of the XAS spectra, are well reproduced by the calculation, which allows for a more detailed discussion of the different features.

Feature A is present in all spectra but slightly shifts and changes spectral shape for the different polarization directions, which is reproduced in the calculation. The calculations show strongly varying contributions of the inequivalent oxygen atoms to the absorption spectra for the three orientations and excitation energies, which can be used to selectively enhance the contributions of specific oxygen

environments as suggested in Ref. 35. In detail, feature A is dominated by absorption at O2 and O3 for $\vec{\varepsilon}_{exc} \parallel \vec{a}$. For $\vec{\varepsilon}_{exc} \parallel \vec{b}$, all oxygen atoms contribute and for $\vec{\varepsilon}_{exc} \parallel \vec{c}$, only O1 and O2 give rise to appreciable intensity. Feature B is most prominent for $\vec{\varepsilon}_{exc} \parallel \vec{b}$ and $\vec{\varepsilon}_{exc} \parallel \vec{c}$ and less pronounced for $\vec{\varepsilon}_{exc} \parallel \vec{a}$. For $\vec{\varepsilon}_{exc} \parallel \vec{c}$, a distinct peak can be found in this region, which can be related to absorption at O3. Conversely, features C and E are most distinct for $\vec{\varepsilon}_{exc} \parallel \vec{a}$ and $\vec{\varepsilon}_{exc} \parallel \vec{c}$ while reduced for $\vec{\varepsilon}_{exc} \parallel \vec{b}$. In the calculations, O2 strongly contributes to feature C for $\vec{\varepsilon}_{exc} \parallel \vec{a}$ and $\vec{\varepsilon}_{exc} \parallel \vec{c}$, while O1 makes the strongest contribution to feature E for $\vec{\varepsilon}_{exc} \parallel \vec{a}$.

Figure 5 shows the measured and calculated coherent contributions of the RIXS spectra for β-Ga_2O_3 for all three polarization directions. To obtain the coherent contributions in the experiment, individual RIXS spectra were extracted from the RIXS maps shown in Fig. 3 by taking horizontal cuts through the maps. These spectra contain both coherent and incoherent contributions, while the calculated spectra contain the coherent part only. In a simple model suggested in Refs. 51 and 52, the incoherent contribution is approximated by a spectrum excited high above the absorption edge (i.e., a non-resonant spectrum), and subsequently, a maximal amount of this incoherent spectrum is subtracted from each RIXS spectrum, without generating negative intensities. This approach is not easily applicable to β-Ga_2O_3 due to its inequivalent O atoms that contribute differently at different excitation energies.[35,37,38] Nevertheless, we have used this procedure to derive an *estimate* for the experimental coherent fraction, as exemplarily shown for two excitation energies in Fig. S1; the result is shown in Fig. 5.
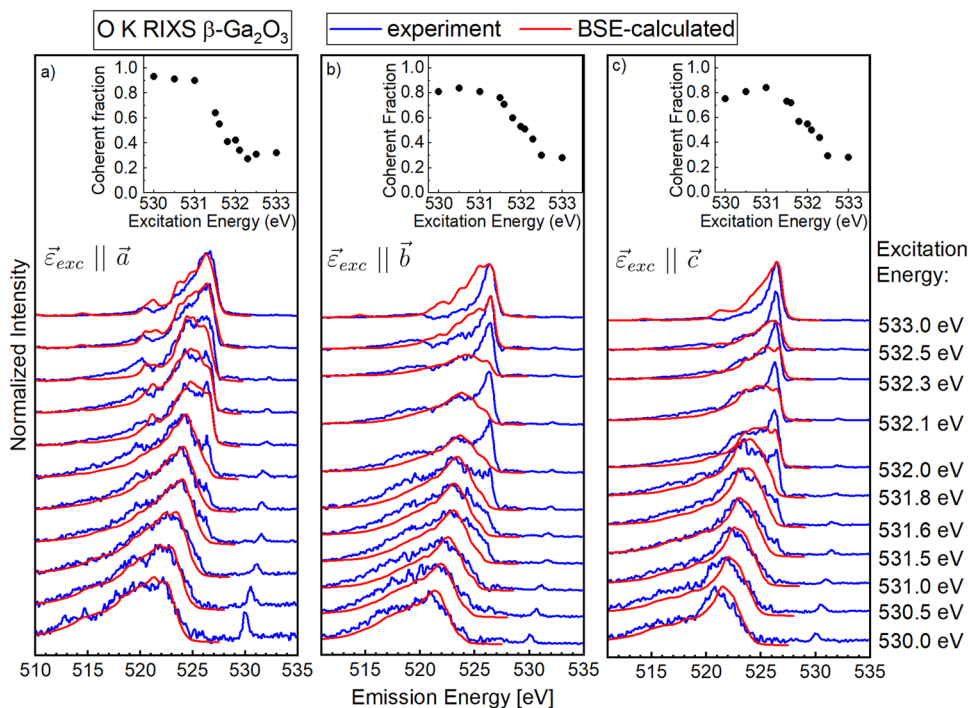
FIG. 5. Coherent contributions of the experimental RIXS spectra compared to calculations at selected excitation energies for a) $\vec{\varepsilon}_{exc} \parallel \vec{a}$, b) $\vec{\varepsilon}_{exc} \parallel \vec{b}$, and c) $\vec{\varepsilon}_{exc} \parallel \vec{c}$. The experimental spectra are normalized to the peak maxima, and the calculated spectra are scaled for the best correspondence to the experiment. The emission energy axes of all calculated spectra were shifted by the same amount to match the feature positions of the experimental spectra. The insets (upper right corners) show the respective coherent fractions (i.e., the percentage of the coherent contribution in the overall spectrum) as a function of the excitation energy.

For all three polarization directions, the following types of features are observed in the experimental spectra: the elastically scattered (Rayleigh) peak, emission features that do not shift as a function of excitation energy, and emission features that exhibit a Raman-like behavior (i.e., their emission energy shifts linearly with excitation energy). Below the absorption edge ($\approx$532 eV), only excitations into "virtual" states are possible and the emission lines shift with Raman behavior. In this excitation-energy region, we find very good agreement between experiment and calculations for all three polarization directions. The spectral shapes change only slightly as a function of excitation energy, but distinct differences are observed between the polarization directions (e.g., the spectra are narrower when $\vec{\varepsilon}_{exc} \parallel \vec{c}$).

Above the absorption edge at $\approx$532 eV, spectral shapes change significantly as a function of excitation energy and no Raman-like shift is observed. While the agreement between experiment and theory is still very good when $\vec{\varepsilon}_{exc} \parallel \vec{a}$, the agreement is poor for $\vec{\varepsilon}_{exc} \parallel \vec{b}$ and $\vec{\varepsilon}_{exc} \parallel \vec{c}$. As discussed above, this is expected due to the inequivalent oxygen atoms. At resonant excitation, they are not equally excited (see Fig. 4) and since our calculation in Fig. 2(b) indicates significant differences between the non-resonant spectra of these oxygen atoms, the experimental non-resonant spectra are no longer good approximations for the incoherent contribution. For excitation below $\approx$532 eV, the coherent contribution dominates the spectra (see the insets) and the error introduced by the approximation of the incoherent contribution is small. Above $\approx$532 eV, the incoherent contribution increases significantly and the error gets much larger. Notably, $\vec{\varepsilon}_{exc} \parallel \vec{a}$ is the exception, where the subtraction of the incoherent contribution works well for all energies. This can be attributed to the fact that, for this polarization, the non-resonant spectra of the inequivalent oxygen atoms are rather similar. Qualitatively, O1 is preferred for $\vec{\varepsilon}_{exc} \parallel \vec{b}$ and $\vec{c}$ with excitation below 535 eV (see Fig. 4) and the non-resonant emission spectra of O1 contain a sharp and intense peak at $\approx$526 eV for these polarizations [see Fig. 2(b)], which then remains after subtraction of the non-resonant spectra shown in Figs. 5(b) and 5(c).

Combining the measured and calculated XAS and XES spectra, we can estimate the one-particle fundamental bandgap of β-Ga$_2$O$_3$. The observed extrema of the emission and absorption spectra do not identify the true band extrema. They only probe the p-type electronic states around the oxygen atoms, and, furthermore, the absorption is redshifted by the presence of the core hole. However, the OCEAN calculations account for these effects. In the calculations, the gap between the absorption and emission spectra is set by the one-particle gap and the BSE excitonic binding in the absorption. DFT calculations typically underestimate the one-particle gap, often by 50% or more, due to the neglect of many-body terms, which can be corrected through GW self-energy calculations.[53] Another limitation of the DFT bandgap is a lack of phonon renormalization, although this is smaller than the self-energy and has the opposite effect, reducing the gap by a few tens to hundreds of meV.[54]

By aligning the calculated spectra to the experimental XAS and XES measurements, we estimate a one-particle gap that includes these effects. This alignment required an adjustment of 2.9 eV on top of the DFT-calculated bandgap of 2.5 eV, giving a true one-particle bandgap of 5.4 eV. The primary source of error in our estimation of the gap is from using only the lowest-order interactions in

the BSE calculations and the limitation of using DFT orbitals. We repeated absorption and non-resonant emission calculations using the r2SCAN exchange–correlation functional[55] and found a corrected one-particle gap of 5.3 eV, leading us to estimate an error range of ±0.2 eV. Reported optical gaps are 0.5–1 eV smaller,[2–8] presumably not only due to (valence) excitonic effects but also possibly due to shortcoming in the Tauc plot approach[56] or differences in sample quality. A previous comparison of x-ray spectra estimated the gap to be 5.0 eV,[36] but that value did not account for the excitonic binding. Our method of determining bandgaps by combining x-ray measurements and calculations can be applied broadly. As an x-ray technique, it is relatively insensitive to surface defects or contamination and can be applied to buried layers of heterostructures and to determine the position of defect or dopant midgap states.

In conclusion, we have presented XES and XAS spectra, as well as RIXS maps, of a β-Ga$_2$O$_3$ single crystal with the polarization of the incoming x-ray photon beam oriented parallel to each of the unit cell vectors. The experimental spectra are compared to spectra calculations corresponding to each experimental configuration using the BSE method in the OCEAN code. The calculations reproduce the main features in the experimental spectra. Most strikingly, significant differences in all spectra are found for the different polarization directions, both in the experiment and in the calculations. These differences are caused by the polarization dependence of the dipole transition matrix elements, as well as which one of the inequivalent O atoms (O1, O2, and O3) is excited. The good correspondence between the calculated and measured spectra demonstrates the capability of using OCEAN to simulate and predict the electronic structure (including an optimized approach to estimate the one-particle fundamental bandgap) not only for β-Ga$_2$O$_3$ but also for other TCOs, including those that have not yet been synthesized or measured.

EXPERIMENTAL METHODS

β-Ga$_2$O$_3$ single crystals in the (010) (of size 10 × 15 × 0.51 mm^3) and (001) (of size 10 × 15 × 0.65 mm^3) orientations were obtained from Novel Crystal Technology, Inc., Tamura Corporation, where they were grown by using the edge-defined film-fed growth method.[57] The samples were doped with Sn to improve their conductivity, resulting in carrier concentrations of 3.6 × 10^{18} cm^{-3} for the (010) crystal and 6.3 × 10^{18} cm^{-3} for the (001) crystal.

Non-resonant XES spectra and RIXS maps were recorded at Beamline 8.0.1 of the Advanced Light Source (ALS), Lawrence Berkeley National Laboratory using our SALSA endstation.[58] The SALSA endstation uses a high-resolution, high-transmission x-ray spectrometer, with an entrance slit-less design, a spherical collecting mirror, a variable line spacing grating, and a soft x-ray CCD.[59] The combined resolving power for the spectrometer and the beamline was set to be better than 1000. The optical axis of the spectrometer was oriented at $(45 \pm 2)°$ relative to the incident photon beam in the plane of the storage ring, with the spectrometer accepting about 0.6° vertically and 1° horizontally. Samples were mounted on the sample holder with an accuracy of ± 1° to align the unit cell vectors ($\vec{a}$ and $\vec{c}$ with the (010) crystal and $\vec{b}$ with the (001) crystal, see Fig. 1) parallel to the polarization $\vec{\varepsilon}_{exc}$ of the exciting photon beam. The emission energy scale was calibrated using the emission energies of BN and CaSO$_4$ reference samples.[60] The excitation energies were

then calibrated using the energy position of the elastically scattered (Rayleigh) line in each spectrum. We approximate an uncertainty of the absolute emission and excitation energy scales of better than ± 0.1 eV. Prior to plotting the experimental spectra, contributions of the higher harmonics of the spectrometer, as well as additional intensities due to, e.g., Wentzel-Druyvesteyn (WD) satellites,[61] were subtracted from the spectra.

COMPUTATIONAL METHODS

The electronic structure and polarization-independent XES spectrum of β-Ga_2O_3 were calculated using WIEN2k version 21.1, which is based on the full-potential augmented plane-wave plus local orbitals (APW + lo) method to solve the Kohn–Sham DFT equations.[44] The generalized gradient approximation (GGA) in the Perdew, Burke, and Ernzerhof (PBE) parameterization[62] was used to approximate the exchange–correlation functional. The product of the smallest muffin tin radius R_{MT} and the largest k-vector K_{max} was set to 8. The self-consistent field (SCF) cycle was run with 1000 k points, while the projected density of state (PDOS) and XES calculations were run with 10 000 k points. The XES spectra were calculated according to the formalism in Refs. 45 and 63. The dipole matrix elements were generated on the basis of the dipole selection rules and then multiplied by the corresponding PDOS and radial transition probability to obtain the spectra.[64]

The polarization-dependent x-ray calculations were performed with the OCEAN code, where the ground-state wave functions were calculated with the pseudopotential-based code Quantum Espresso.[65] Pseudopotentials were taken from the PseudoDojo collection,[66] version 0.4 stringent, and were constructed using the optimized norm-conserving Vanderbilt method.[67] The plane-wave cutoff was set to 122 Ryd, and, as in Wien2k, the GGA with the PBE parameterization was used. The number of DFT conduction band states included as final states in the BSE calculations was chosen such that they span ~40 eV above the conduction band minimum. A series of convergence tests was performed to determine the optimal k-point and x-point grids for calculation of the final states, which were taken as $8 \times 8 \times 5$ and $14 \times 14 \times 12$, respectively. A $4 \times 4 \times 3$ k-point grid was sufficient for the SCF cycle. The number of conduction bands for the screening calculations was chosen such that they span ~150 eV above the conduction band minimum. The energies of the calculated emission and absorption were determined from the quasiparticle energies of the conduction or valence bands in the DFT calculation and the electron–hole interactions within BSE. The relative energy shifts of the oxygen 1s orbital between the three unique oxygen sites were calculated,[68] but a single fit parameter was used to align all calculated x-ray spectra to the experiment. In addition, per discussion above, a bandgap correction of 2.9 eV was necessary to simultaneously align theory to experiment in both absorption and emission.

A small Lorentzian broadening [(0.2 eV full-width at half maximum (FWHM)] for the core–hole lifetime is included in the spectra, to which Gaussian (FWHM of 0.5 eV) and Lorentzian (FWHM of 0.1 eV) broadening was further applied when comparing the calculations with the experiment. A stretch factor of 5% was applied to the excitation energy axis of the XAS spectra calculated using OCEAN. The crystal structure was obtained from the Crystallography Open Database[69] (entry 2 004 987[70]), and the structure from the Materials

Project[71] (material ID md-886) gave very similar results. The OCEAN input file is given in the supplementary material.

SUPPLEMENTARY MATERIAL

The supplementary material is available free of charge: the OCEAN input file and subtraction of the incoherent fraction.

AUTHOR DECLARATIONS

Conflict of Interest

The authors have no conflicts to disclose.

Author Contributions

Elizaveta Pyatenko: Data curation (equal); Formal analysis (equal); Investigation (equal); Writing – original draft (equal). **John Vinson**: Conceptualization (equal); Formal analysis (equal); Investigation (equal); Methodology (equal); Software (lead); Supervision (supporting); Validation (equal); Writing – review & editing (equal). **Dirk Hauschild**: Data curation (equal); Formal analysis (supporting); Investigation (equal); Supervision (supporting); Validation (equal); Writing – review & editing (supporting). **Constantin Wansorra**: Data curation (equal); Investigation (supporting); Writing – review & editing (supporting). **Wanli Yang**: Data curation (supporting); Investigation (supporting); Writing – review & editing (supporting). **Monika Blum**: Data curation (supporting); Investigation (supporting); Writing – review & editing (supporting). **Clemens Heske**: Conceptualization (equal); Formal analysis (supporting); Methodology (equal); Supervision (equal); Validation (equal); Writing – review & editing (equal). **Lothar Weinhardt**: Conceptualization (equal); Data curation (equal); Formal analysis (equal); Investigation (equal); Methodology (equal); Supervision (equal); Writing – review & editing (equal).

DATA AVAILABILITY

The data that support the findings of this study are available from the corresponding author upon reasonable request.

REFERENCES

[1]J. Y. Tsao, S. Chowdhury, M. A. Hollis, D. Jena, N. M. Johnson, K. A. Jones, R. J. Kaplar, S. Rajan, C. G. Van de Walle, E. Bellotti, C. L. Chua, R. Collazo, M. E. Coltrin, J. A. Cooper, K. R. Evans, S. Graham, T. A. Grotjohn, E. R. Heller,

21 July 2025 15:15:09

M. Higashiwaki, M. S. Islam, P. W. Juodawlkis, M. A. Khan, A. D. Koehler, J. H. Leach, U. K. Mishra, R. J. Nemanich, R. C. N. Pilawa-Podgurski, J. B. Shealy, Z. Sitar, M. J. Tadjer, A. F. Witulski, M. Wraback, and J. A. Simmons, "Ultrawide-bandgap semiconductors: Research opportunities and challenges," Adv. Electr. Mater. **4**(1), 1600501 (2018).

[2]S. Garud, N. Gampa, T. G. Allen, R. Kotipalli, D. Flandre, M. Batuk, J. Hadermann, M. Meuris, J. Poortmans, A. Smets, and B. Vermang, "Surface passivation of CIGS solar cells using gallium oxide," Phys. Status Solidi A **215**(7), 1700826 (2018).

[3]W. Witte, S. Paetel, R. Menner, A. Bauer, and D. Hariskos, "The application of sputtered gallium oxide as buffer for Cu(In, Ga)Se₂ solar cells," Phys. Status Solidi RRL **15**(9), 2100180 (2021).

[4]*Gallium Oxide: Materials Properties, Crystal Growth, and Devices*, Springer Series in Materials Science, edited by M. Higashiwaki, and S. Fujita (Springer International Publishing, Cham, 2020), Vol. 293.

[5]T. Onuma, S. Saito, K. Sasaki, T. Masui, T. Yamaguchi, T. Honda, and M. Higashiwaki, "Valence band ordering in β-Ga₂O₃ studied by polarized transmittance and reflectance spectroscopy," Jpn. J. Appl. Phys. **54**(11), 112601 (2015).

[6]H. H. Tippins, "Optical absorption and photoconductivity in the band edge of β-Ga₂O₃," Phys. Rev. **140**(1A), A316–A319 (1965).

[7]M. Orita, H. Ohta, M. Hirano, and H. Hosono, "Deep-ultraviolet transparent conductive β-Ga₂O₃ thin films," Appl. Phys. Lett. **77**(25), 4166–4168 (2000).

[8]H. He, R. Orlando, M. A. Blanco, R. Pandey, E. Amzallag, I. Baraille, and M. Rérat, "First-principles study of the structural, electronic, and optical properties of Ga₂O₃ in its monoclinic and hexagonal phases," Phys. Rev. B **74**(19), 195123 (2006).

[9]M. H. Wong, O. Bierwagen, R. J. Kaplar, and H. Umezawa, "Ultrawide-bandgap Semiconductors: An overview," J. Mater. Res. **36**(23), 4601–4615 (2021).

[10]E. Pyatenko, D. Hauschild, V. Mikhnych, R. Edla, R. Steininger, D. Hariskos, W. Witte, M. Powalla, C. Heske, and L. Weinhardt, "Rb diffusion and oxide removal at the RbF-treated Ga₂O₃/Cu(in,Ga)Se₂ interface in thin-film solar cells," ACS Appl. Mater. Interfaces **15**(45), 53113–53121 (2023).

[11]W. Witte, W. Hempel, S. Paetel, R. Menner, and D. Hariskos, "Influence of sputtered gallium oxide as buffer or high-resistive layer on performance of Cu(In, Ga)Se₂-based solar cells," J. Mater. Res. **37**(11), 1825–1834 (2022).

[12]M. Higashiwaki, K. Sasaki, A. Kuramata, T. Masui, and S. Yamakoshi, "Gallium oxide (Ga₂O₃) metal-semiconductor field-effect transistors on single-crystal β-Ga₂O₃ (010) substrates," Appl. Phys. Lett. **100**(1), 013504 (2012).

[13]M. Higashiwaki, K. Sasaki, A. Kuramata, T. Masui, and S. Yamakoshi, "Development of gallium oxide power devices," Phys. Status Solidi A **211**(1), 21–26 (2014).

[14]A.-C. Liu, C.-H. Hsieh, C. Langpoklakpam, K. J. Singh, W.-C. Lee, Y.-K. Hsiao, R.-H. Horng, H.-C. Kuo, and C.-C. Tu, "State-of-the-Art β-Ga₂O₃ field-effect transistors for power electronics," ACS Omega **7**(41), 36070–36091 (2022).

[15]A. J. Green, J. Speck, G. Xing, P. Moens, F. Allerstam, K. Gumaelius, T. Neyer, A. Arias-Purdue, V. Mehrotra, A. Kuramata, K. Sasaki, S. Watanabe, K. Koshi, J. Blevins, O. Bierwagen, S. Krishnamoorthy, K. Leedy, A. R. Arehart, A. T. Neal, S. Mou, S. A. Ringel, A. Kumar, A. Sharma, K. Ghosh, U. Singisetti, W. Li, K. Chabak, K. Liddy, A. Islam, S. Rajan, S. Graham, S. Choi, Z. Cheng, and M. Higashiwaki, "β-Gallium oxide power electronics," APL Mater. **10**(2), 029201 (2022).

[16]Y. Kokubun, K. Miura, F. Endo, and S. Nakagomi, "Sol-gel prepared β-Ga₂O₃ thin films for ultraviolet photodetectors," Appl. Phys. Lett. **90**(3), 031912 (2007).

[17]X. Chen, F.-F. Ren, J. Ye, and S. Gu, "Gallium oxide-based solar-blind ultraviolet photodetectors," Semicond. Sci. Technol. **35**(2), 023001 (2020).

[18]D. Y. Guo, Z. P. Wu, Y. H. An, X. C. Guo, X. L. Chu, C. L. Sun, L. H. Li, P. G. Li, and W. H. Tang, "Oxygen vacancy tuned ohmic-Schottky conversion for enhanced performance in β-Ga₂O₃ solar-blind ultraviolet photodetectors," Appl. Phys. Lett. **105**(2), 023507 (2014).

[19]J. Wang, L. Ye, X. Wang, H. Zhang, L. Li, C. Kong, and W. Li, "High transmittance Ga₂O₃ thin films deposited by magnetron sputtering and post-annealing for solar-blind ultraviolet photodetector," J. Alloys Compd. **803**, 9–15 (2019).

[20]M. Ogita, K. Higo, Y. Nakanishi, and Y. Hatanaka, "Ga₂O₃ thin film for oxygen sensor at high temperature," Appl. Surf. Sci. **175–176**, 721–725 (2001).

[21]H. Zhai, Z. Wu, and Z. Fang, "Recent progress of Ga₂O₃-based gas sensors," Ceram. Int. **48**(17), 24213–24233 (2022).

[22]R. Pandeeswari and B. G. Jeyaprakash, "High sensing response of β-Ga₂O₃ thin film towards ammonia vapours: Influencing factors at room temperature," Sens. Actuators, B **195**, 206–214 (2014).

[23]K. Nakagawa, M. Okamura, N. Ikenaga, T. Suzuki, K. Nakagawa, M. Okamura, T. Suzuki, T. Kobayashi, and T. Kobayashi, "Dehydrogenation of ethane over gallium oxide in the presence of carbon dioxide," Chem. Commun. **1998**(9), 1025–1026.

[24]C.-T. Shao, W.-Z. Lang, X. Yan, and Y.-J. Guo, "Catalytic performance of gallium oxide based-catalysts for the propane dehydrogenation reaction: Effects of support and loading amount," RSC Adv. **7**(8), 4710–4723 (2017).

[25]A. Lowry, "High-voltage gallium oxide devices for space power electronics, phase I," https://techport.nasa.gov/view/113274 (accessed 10/21/2023).

[26]D. A. Bauman, A. I. Borodkin, A. A. Petrenko, D. I. Panov, A. V. Kremleva, V. A. Spiridonov, D. A. Zakgeim, M. V. Silnikov, M. A. Odnoblyudov, A. E. Romanov, and V. E. Bougrov, "On improving the radiation resistance of gallium oxide for space applications," Acta Astronaut. **180**, 125–129 (2021).

[27]R. Roy, V. G. Hill, and E. F. Osborn, "Polymorphism of Ga₂O₃ and the system Ga₂O₃–H₂O," J. Am. Chem. Soc. **74**, 719 (1952).

[28]N. Ueda, H. Hosono, R. Waseda, and H. Kawazoe, "Anisotropy of electrical and optical properties in β-Ga₂O₃ single crystals," Appl. Phys. Lett. **71**(7), 933–935 (1997).

[29]F. Ricci, F. Boschi, A. Baraldi, A. Filippetti, M. Higashiwaki, A. Kuramata, V. Fiorentini, and R. Fornari, "Theoretical and experimental investigation of optical absorption anisotropy in β-Ga₂O₃," J. Phys.: Condens. Matter **28**(22), 224005 (2016).

[30]T. Matsumoto, M. Aoki, A. Kinoshita, and T. Aono, "Absorption and reflection of vapor grown single crystal platelets of β-Ga₂O₃," Jpn. J. Appl. Phys. **13**(10), 1578–1582 (1974).

[31]M. Mohamed, C. Janowitz, I. Unger, R. Manzke, Z. Galazka, R. Uecker, R. Fornari, J. R. Weber, J. B. Varley, and C. G. Van de Walle, "The electronic structure of β-Ga₂O₃," Appl. Phys. Lett. **97**(21), 211903 (2010).

[32]M. Mohamed, I. Unger, C. Janowitz, R. Manzke, Z. Galazka, R. Uecker, and R. Fornari, "The surface band structure of β-Ga₂O₃," J. Phys.: Conf. Ser. **286**, 012027 (2011).

[33]C. Janowitz, V. Scherer, M. Mohamed, A. Krapf, H. Dwelk, R. Manzke, Z. Galazka, R. Uecker, K. Irmscher, R. Fornari, M. Michling, D. Schmeißer, J. R. Weber, J. B. Varley, and C. G. V. D. Walle, "Experimental electronic structure of In₂O₃ and Ga₂O₃," New J. Phys. **13**(8), 085014 (2011).

[34]M. Mohamed, K. Irmscher, C. Janowitz, Z. Galazka, R. Manzke, and R. Fornari, "Schottky barrier height of Au on the transparent semiconducting oxide β-Ga₂O₃," Appl. Phys. Lett. **101**(13), 132106 (2012).

[35]C. Cocchi, H. Zschiesche, D. Nabok, A. Mogilatenko, M. Albrecht, Z. Galazka, H. Kirmse, C. Draxl, and C. T. Koch, "Atomic signatures of local environment from core-level spectroscopy in β-Ga₂O₃," Phys. Rev. B **94**(7), 075147 (2016).

[36]J. E. N. Swallow, C. Vorwerk, P. Mazzolini, P. Vogt, O. Bierwagen, A. Karg, M. Eickhoff, J. Schörmann, M. R. Wagner, J. W. Roberts, P. R. Chalker, M. J. Smiles, P. Murgatroyd, S. A. Razek, Z. W. Lebens-Higgins, L. F. J. Piper, L. A. H. Jones, P. K. Thakur, T.-L. Lee, J. B. Varley, J. Furthmüller, C. Draxl, T. D. Veal, and A. Regoutz, "Influence of polymorphism on the electronic structure of Ga₂O₃," Chem. Mater. **32**(19), 8460–8470 (2020).

[37]C. W. Vorwerk, "Theoretical spectroscopy of Ga₂O₃," Doctoral thesis, Humbolt-Universität zu Berlin, Berlin, Germany, 2020.

[38]C. Vorwerk, F. Sottile, and C. Draxl, "All-electron many-body approach to resonant inelastic X-ray scattering," Phys. Chem. Chem. Phys. **24**(29), 17439–17448 (2022).

[39]H. Peelaers and C. G. Van de Walle, "Brillouin zone and band structure of β-Ga₂O₃," Phys. Status Solidi B **252**(4), 828–832 (2015).

[40]K. Momma and F. Izumi, "*VESTA 3* for three-dimensional visualization of crystal, volumetric and morphology data," J. Appl. Crystallogr. **44**(6), 1272–1276 (2011).

[41]V. I. Grebennikov, Yu. A. Babanov, and O. B. Sokolov, "Extra-atomic relaxation and X-ray spectra of narrow-band metals. I. Formalism," Phys. Status Solidi B **79**(2), 423–432 (1977).

[42]G. D. Mahan, "Final-state potential in x-ray spectra," Phys. Rev. B **21**(4), 1421–1431 (1980).

21 July 2025 15:15:09

[43] U. Von Barth and G. Grossmann, "Dynamical effects in X-ray spectra and the final-state rule," Phys. Rev. B **25**(8), 5150–5179 (1982).

[44] P. Blaha, K. Schwarz, F. Tran, R. Laskowski, G. K. H. Madsen, and L. D. Marks, "WIEN2k: An APW+lo program for calculating the properties of solids," J. Chem. Phys. **152**(7), 074101 (2020).

[45] K. Schwarz, A. Neckel, and J. Nordgren, "On the X-ray emission spectra from FeAl," J. Phys. F: Met. Phys. **9**(12), 2509–2521 (1979).

[46] J. Vinson, J. J. Rehr, J. J. Kas, and E. L. Shirley, "Bethe-Salpeter equation calculations of core excitation spectra," Phys. Rev. B **83**(11), 115106 (2011).

[47] J. Vinson, "Advances in the ocean-3 spectroscopy package," Phys. Chem. Chem. Phys. **24**(21), 12787–12803 (2022).

[48] C. McGuinness, C. B. Stagarescu, P. J. Ryan, J. E. Downes, D. Fu, K. E. Smith, and R. G. Egdell, "Influence of shallow core-level hybridization on the electronic structure of post-transition-metal oxides studied using soft X-ray emission and absorption," Phys. Rev. B **68**(16), 165104 (2003).

[49] A. Qteish, A. I. Al-Sharif, M. Fuchs, M. Scheffler, S. Boeck, and J. Neugebauer, "Role of semicore states in the electronic structure of group-III nitrides: An exact-exchange study," Phys. Rev. B **72**(15), 155317 (2005).

[50] Y. Ma, N. Wassdahl, P. Skytt, J. Guo, J. Nordgren, P. D. Johnson, J.-E. Rubensson, T. Boske, W. Eberhardt, and S. D. Kevan, "Soft-x-ray resonant inelastic scattering at the C K edge of diamond," Phys. Rev. Lett. **69**(17), 2598 (1992).

[51] J. Lüning, J.-E. Rubensson, C. Ellmers, S. Eisebitt, and W. Eberhardt, "Site-and symmetry-projected band structure measured by resonant inelastic soft x-ray scattering," Phys. Rev. B **56**(20), 13147–13150 (1997).

[52] D. Eich, O. Fuchs, U. Groh, L. Weinhardt, R. Fink, E. Umbach, C. Heske, A. Fleszar, W. Hanke, E. K. U. Gross, C. Bostedt, T. Von Buuren, N. Franco, L. J. Terminello, M. Keim, G. Reuscher, H. Lugauer, and A. Waag, "Resonant inelastic soft X-ray scattering of Be chalcogenides," Phys. Rev. B **73**(11), 115212 (2006).

[53] F. Aryasetiawan and O. Gunnarsson, "The GW method," Rep. Prog. Phys. **61**(3), 237 (1998).

[54] F. Giustino, "Electron-phonon interactions from first principles," Rev. Mod. Phys. **89**(1), 015003 (2017).

[55] J. W. Furness, A. D. Kaplan, J. Ning, J. P. Perdew, and J. Sun, "Accurate and numerically efficient r2SCAN meta-generalized gradient approximation," J. Phys. Chem. Lett. **11**(19), 8208–8215 (2020).

[56] Z. Chen, T. F. Jaramillo, T. G. Deutsch, A. Kleiman-Shwarscstein, A. J. Forman, N. Gaillard, R. Garland, K. Takanabe, C. Heske, M. Sunkara, E. W. McFarland, K. Domen, E. L. Miller, J. A. Turner, and H. N. Dinh, "Accelerating materials development for photoelectrochemical hydrogen production: Standards for methods, definitions, and reporting protocols," J. Mater. Res. **25**(1), 3–16 (2010).

[57] H. Aida, K. Nishiguchi, H. Takeda, N. Aota, K. Sunakawa, and Y. Yaguchi, "Growth of β-Ga₂O₃ single crystals by the edge-defined, film fed growth method," Jpn. J. Appl. Phys. **47**(11R), 8506–8509 (2008).

[58] M. Blum, L. Weinhardt, O. Fuchs, M. Bär, Y. Zhang, M. Weigand, S. Krause, S. Pookpanratana, T. Hofmann, W. Yang, J. D. Denlinger, E. Umbach, and C. Heske, "Solid and liquid spectroscopic analysis (SALSA) – A soft x-ray spectroscopy endstation with a novel flow-through liquid cell," Rev. Sci. Instrum. **80**(12), 123102 (2009).

[59] O. Fuchs, L. Weinhardt, M. Blum, M. Weigand, E. Umbach, M. Bär, C. Heske, J. Denlinger, Y.-D. Chuang, W. McKinney, Z. Hussain, E. Gullikson, M. Jones, P. Batson, B. Nelles, and R. Follath, "High-resolution, high-transmission soft x-ray spectrometer for the study of biological samples," Rev. Sci. Instrum. **80**(6), 063103 (2009).

[60] L. Weinhardt, D. Hauschild, R. Steininger, N. Jiang, M. Blum, W. Yang, and C. Heske, "Sulfate speciation analysis using soft X-ray emission spectroscopy," Anal. Chem. **93**(23), 8300–8308 (2021).

[61] J.-E. Rubensson, L. Petersson, N. Wassdahl, M. Bäckström, J. Nordgren, O. M. Kvalheim, and R. Manne, "Radiative decay of multiply excited core hole states in H₂O," J. Chem. Phys. **82**(10), 4486–4491 (1985).

[62] J. P. Perdew, K. Burke, and M. Ernzerhof, "Generalized gradient approximation made simple," Phys. Rev. Lett. **77**(18), 3865–3868 (1996).

[63] K. Schwarz and E. Wimmer, "Electronic structure and X-ray emission spectra of YS in comparison with NbC," J. Phys. F: Met. Phys. **10**(5), 1001–1012 (1980).

[64] P. Blaha, K. Schwarz, G. K. H. Madsen, D. Kvasnicka, J. Luitz, R. Laskowski, F. Tran, and L. D. Marks, WIEN2k an augmented plane wave plus local orbitals program for calculating crystal properties user's guide, WIEN2k_23.1, 2023.

[65] P. Giannozzi, S. Baroni, N. Bonini, M. Calandra, R. Car, C. Cavazzoni, D. Ceresoli, G. L. Chiarotti, M. Cococcioni, I. Dabo, A. Dal Corso, S. De Gironcoli, S. Fabris, G. Fratesi, R. Gebauer, U. Gerstmann, C. Gougoussis, A. Kokalj, M. Lazzeri, L. Martin-Samos, N. Marzari, F. Mauri, R. Mazzarello, S. Paolini, A. Pasquarello, L. Paulatto, C. Sbraccia, S. Scandolo, G. Sclauzero, A. P. Seitsonen, A. Smogunov, P. Umari, and R. M. Wentzcovitch, "QUANTUM ESPRESSO: A modular and open-source software project for quantum simulations of materials," J. Phys.: Condens. Matter **21**(39), 395502 (2009).

[66] M. J. van Setten, M. Giantomassi, E. Bousquet, M. J. Verstraete, D. R. Hamann, X. Gonze, and G.-M. Rignanese, "The PseudoDojo: Training and grading a 85 element optimized norm-conserving pseudopotential table," Comput. Phys. Commun. **226**, 39–54 (2018).

[67] D. R. Hamann, "Optimized norm-conserving Vanderbilt pseudopotentials," Phys. Rev. B **88**(8), 085117 (2013).

[68] J. Vinson and E. L. Shirley, "Fast, efficient, and accurate dielectric screening using a local real-space approach," Phys. Rev. B **103**(24), 245143 (2021).

[69] S. Gražulis, A. Daškevič, A. Merkys, D. Chateigner, L. Lutterotti, M. Quirós, N. R. Serebryanaya, P. Moeck, R. T. Downs, and A. Le Bail, "Crystallography Open Database (COD): An open-access collection of crystal structures and platform for world-wide collaboration," Nucleic Acids Res. **40**(D1), D420–D427 (2012).

[70] J. Åhman, G. Svensson, and J. Albertsson, "A reinvestigation of β-gallium oxide," Acta Crystallogr., Sect. C **52**(6), 1336–1338 (1996).

[71] A. Jain, S. P. Ong, G. Hautier, W. Chen, W. D. Richards, S. Dacek, S. Cholia, D. Gunter, D. Skinner, G. Ceder, and K. A. Persson, "Commentary: The materials project: A materials genome approach to accelerating materials innovation," APL Mater. **1**(1), 011002 (2013).